Journal of Power Sources 190 (2009) 563–572

Contents lists available at ScienceDirect

Journal of Power Sources

journal homepage: www.elsevier.com/locate/jpowsour

Magnesium ion-conducting gel polymer electrolytes dispersed with nanosized magnesium oxide

G.P. Pandey[a,b], R.C. Agrawal[b], S.A. Hashmi[a,*]

[a] Department of Physics & Astrophysics, University of Delhi, Delhi 110007, India
[b] Solid State Ionics Research Laboratory, School of Studies in Physics, Pt. Ravishankar Shukla University, Raipur 492010, C.G., India

ARTICLE INFO

Article history:
Received 9 November 2008
Received in revised form 19 December 2008
Accepted 8 January 2009
Available online 30 January 2009

Keywords:
Gel polymer electrolyte
Nanocomposite
Magnesium ion conductor
Magnesium batteries
AC impedance spectroscopy
Cyclic voltammetry

ABSTRACT

Experimental investigations are performed on novel magnesium ion-conducting gel polymer electrolyte nanocomposites based on poly(vinylidene fluoride-co-hexafluoropropylene) (PVdF-HFP), dispersed with nanosized magnesium oxide (MgO) particles. The nanocomposite materials are in the form of free-standing films. Various physical and electrochemical analyses demonstrate promising characteristics of these films, suitable as electrolytes in rechargeable magnesium batteries. The optimized material with 3 wt.% MgO offers a maximum electrical conductivity of $\sim 8 \times 10^{-3}$ S cm^{-1} at room temperature ($\sim$25 °C) with good thermal and electrochemical stabilities. The ion/filler–polymer interactions and possible conformational changes in host polymer PVdF-HFP due to the liquid electrolyte entrapment and dispersion of nanosized MgO are examined by Fourier transform infrared (FTIR), X-ray diffraction (XRD) and scanning electron microscopic (SEM) methods. The Mg^{2+} ion conduction in the gel film is confirmed from the cyclic voltammetry, impedance spectroscopy and transport number measurements. The Mg^{2+} ion transport number (t_+) is enhanced substantially and found to have a maximum of $\sim$0.44 for the addition of 10 wt.% MgO nanoparticles. The enhancement in t_+ is explained on the basis of the formation of space-charge regions due to the presence of MgO:Mg^{2+}-like species, that supports Mg^{2+} ion motion.

1. Introduction

The research and development of polymer electrolyte based batteries with high specific energy, good reliability and safety has been an active area for the past three decades [1–3]. Advances in microelectronic industry, especially mobile phones and portable computers, have created a demand for new and improved power sources. Presently, world-wide efforts are directed towards the development of advanced battery technologies based on lithium negative electrodes (anode). To date, the rechargeable lithium ion battery has been one of the best choices in view of specific capacity and cyclic stability [4]. However, rechargeable lithium metal batteries with high specific power or energy are still unavailable in the market. These batteries are relatively expensive and suffer from some safety limitations. Hence, new rechargeable battery systems are required which can be made of cheap and environmental friendly materials.

Recently, the magnesium-based rechargeable battery system has attracted attention due to its performance capabilities, which are expected to be close to those of lithium-based rechargeable batteries [5–7]. Magnesium is one of the ideal materials for the negative electrode for practical batteries because it has low electrochemical equivalence ($\sim$12.15 g eq^{-1}), considerably negative electrode potential (−2.3 V vs. SHE), low cost due to natural abundance, and greater safer than lithium. Aurbach et al. [8] have developed a prototype high-capacity rechargeable magnesium battery using electrolyte solutions based on Mg organohaloaluminate salts. The same group reported that Chevrel phases Mo_6T_8 (T = S, Se) can insert Mg ions reversibly and can be used as practical cathode materials for rechargeable Mg-batteries [9]. Despite these studies, however, development of rechargeable Mg-batteries has not be accelerated mainly due to the lower reversibility of the Mg electrode/electrolyte charge transfer and the lack of suitable Mg^{2+} ion-conducting non-aqueous electrolytes [10,11]. Recently, the development of solid-state Mg^{2+} ion-conducting electrolytes has become one of the important issues to realize rechargeable, solid-state Mg-batteries.

Gel polymer electrolytes, an excellent substitute for liquid electrolytes, continue to attract research interest due to properties which make them suitable for application in solid-state electrochemical devices, e.g., rechargeable batteries, supercapacitors, etc. [12,13]. Such gel electrolytes are examined mostly for use in lithium systems. Mg^{2+} ion-conducting gel polymer electrolytes are not widely reported except a few systems [14–16]. Few solid-state rechargeable magnesium batteries using polymer gel electrolytes have been reported in literature [17,18]. Gel polymer electrolytes

* Corresponding author. Tel.: +91 1127604881; fax: +91 1127667061.
E-mail address: sahashmi@physics.du.ac.in (S.A. Hashmi).

0378-7753/$ – see front matter © 2009 Elsevier B.V. All rights reserved.
doi:10.1016/j.jpowsour.2009.01.057

have some important advantages over liquid electrolytes in that the risk of leakage is reduced, and electrode interfacial contact can be maintained during volumetric changes associated with charge and discharge cycling of the battery. The ability of gel electrolytes to act as both the separator and the electrolyte leads to easy fabrication and allows the possibility of miniaturized devices. However, the main drawback associated with these materials is the tendency to flow, which is deleterious in terms of decay in conductivity and, particularly, in battery reliability and safety. This is obviously a limitation with present gel polymer electrolyte systems and various approaches are under consideration to assure membrane integrity during operation and storage.

The dispersion of nanosized ceramic filler particles, e.g., Al_2O_3, SiO_2, TiO_2, is one of the most reported approaches to improve the mechanical as well as the electrochemical and transport properties of polymer/gel electrolytes [19–21]. In general, the ceramic fillers are broadly classified into two categories, namely, active and passive fillers. The active component materials participate in the conduction process, e.g., Li_2N, $LiAl_2O_3$ are active fillers for Li^+ ion-conducting systems. Passive fillers such as Al_2O_3, SiO_2 or TiO_2 are not directly involved in the ion transport process. Such fillers have also been incorporated into gel electrolytes in order to preserve a porous structure that maximizes the adsorption of liquid electrolyte [22] and to reduce the risk of leakage [23–25].

In the present study, the effect of adding of a nanosized active filler MgO to a PVdF-HFP based Mg^{2+} ion-conducting gel polymer electrolyte is investigated by means of various physical techniques, namely, X-ray diffraction, thermal analysis, infrared spectroscopy, complex impedance analysis, cyclic voltammetry, and conductivity and transport number measurements. The gel polymer electrolyte nanocomposite is found to be a thermally and electrochemically stable material for application in power sources such as magnesium batteries.

2. Experimental

2.1. Materials

The copolymer, poly(vinylidene fluoride-hexafluoropropylene) (PVdF-HFP; average molecular weight 400 000), ethylene carbonate (EC), propylene carbonate (PC), magnesium perchlorate [$Mg(ClO_4)_2$] and the nanosized filler magnesium oxide (MgO; particle size <100 nm) were obtained from Aldrich and used without further purification. The intermediate solvent tetrahydrofuran (THF) was purchased from Merck, India. A solution cast method was used to prepare gel polymer electrolyte nanocomposite films. In this process, the liquid electrolyte was first prepared by dissolving 1 M $Mg(ClO)_4$ in a mixture of EC and PC (1:1, v/v). The host polymer PVdF-HFP was separately dissolved in THF by stirring magnetically at ~50 °C and an appropriate amount (~20 wt.% with respect to the liquid electrolyte for all samples) was mixed in liquid electrolyte. To prepare a gel polymer electrolyte nanocomposite, MgO nanoparticles in different weight ratios from 0 to 20 wt.% with respect to polymer weight were dispersed. The mixtures were then stirred thoroughly for ~10 h and proper filler dispersion was ensured by keeping the mixture in an ultrasonic bath for about 30 min. Finally, the mixture was poured into glass petri dishes and allowed to evaporate the intermediate solvent, THF, to obtain solid-like, free-standing, nanocomposite films of thickness ~300–400 μm.

Circular discs (area = 1.1 cm^2) of magnesium electrodes were obtained by palletising the magnesium powder purchased from Aldrich. These discs were polished with successive grades of emery paper to a smooth finish then washed thoroughly in acetone and dried.

2.2. Instrumentation

The thermal stability of gel polymer electrolyte nanocomposites was tested by thermo-gravimetric analysis (TGA) and differential scanning calorimetry (DSC). TGA was carried out from room temperature to 475 °C under a dynamic dry nitrogen atmosphere at a heating rate of 10 °C min^{-1} using a PerkinElmer TGA system (TGA7). DSC was performed from −90 to 85 °C at a heating rate of 10 °C min^{-1} in a static Nitrogen atmosphere with the help of a DSC system of TA Instruments (Model: Q100). Morphological studies of the gel nanocomposite films were carried out with a scanning electron microscope (JEOL, JSM 5600) and an atomic force microscope (VEECO, USA, model: DI-CP-II). The SEM micrographs were taken at low vacuum after sputtering the samples with gold to prepare conductive surfaces. X-ray diffraction patterns of the films were recorded using a Philips X-ray diffractometer with Cu Kα radiation in the Bragg angle (2θ) range from 10 to 60°. The FTIR spectra were recorded with a PerkinElmer FTIR spectrophotometer.

The electrical conductivities of the gel films were evaluated by means of AC impedance spectroscopy using a LCR Hi-Tester (Model: 3522-50, HIOKI, Japan) over the frequency range from 1 Hz to 100 kHz at a signal level of 10 mV. Conductivity measurements were obtained by sandwiching the films between two stainless-steel (SS) foils over the range of 0–80 °C. Comparative cyclic voltammetric studies were performed on symmetric cells, in which the gel nanocomposite was sandwiched between SS and Mg electrodes, using an electrochemical analyzer (Model: CHI 608C, CH Instruments, USA) at a scan rate of 5 m V s^{-1}. The electrochemical stabilities of the electrolyte films were evaluated by means of linear sweep voltammetry using stainless steel as the working electrode and a Mg disc as combined counter and the reference electrodes.

The total ionic transport number (t_{ion}) was obtained by the polarization technique [26]. In this technique, a SS|gel nanocomposite|SS cell was polarized by applying a step potential of 1.0 V and the resulting potentiostatic current was monitored as a function of time. Stainless steel (SS) acted as blocking electrodes for the above cell. The 't_{ion}' was evaluated using the formula:

$$t_{ion} = \frac{i_T - i_e}{i_T} \quad (1)$$

where i_T and i_e are total and residual current, respectively. The Mg^{2+} ions transport number (t_+) of each gel electrolyte was evaluated using a combination of AC impedance spectroscopy and DC polarization studies on a Mg|gel nanocomposite|Mg cell according to the method of Evans et al. [27].

3. Results and discussion

3.1. Structural studies

The XRD patterns of the PVdF-HFP, filler-free polymer gel electrolyte and the gel polymer electrolyte nanocomposite films are shown in Fig. 1. The XRD pattern of the PVdF-HFP film shows the typical characteristic of a semi-crystalline microstructure, i.e., the co-existence of mixed crystalline and amorphous regions with predominant peaks at 2θ = 14.6, 17, 20, 26.6 and 38° (Fig. 1a). The X-ray diffractogram of the filler-free gel polymer electrolyte shows a broadened peak between 10 and 30° (Fig. 1b). The PVdF-HFP peak at ~27° is masked in the broad peak and the intense peak at ~38° disappears. These changes reveal clearly that the gel polymer electrolyte is predominantly amorphous and its crystallinity is depressed due to the addition of liquid electrolyte. This indicates that the liquid electrolyte solution most likely blends with the PVdF-HFP at the molecular level and functions as a plasticizer for the polymer. The diffractogram of the gel polymer electrolyte nanocomposite film shows the characteristic peaks of

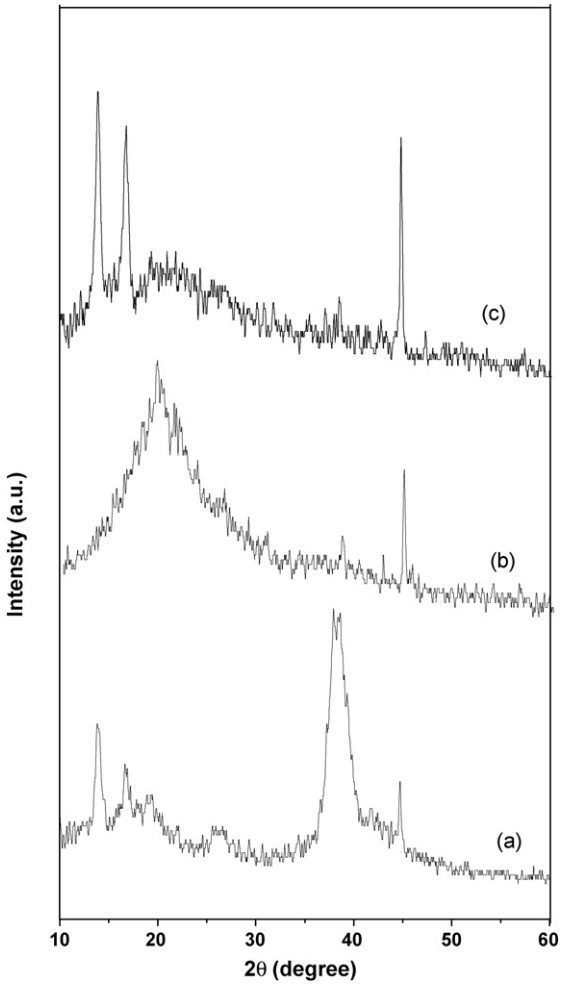

Fig. 1. XRD patterns of PVdF-HFP film (a) and gel polymer electrolyte films containing: 0 wt.% MgO (b) and 10 wt.% MgO (c).

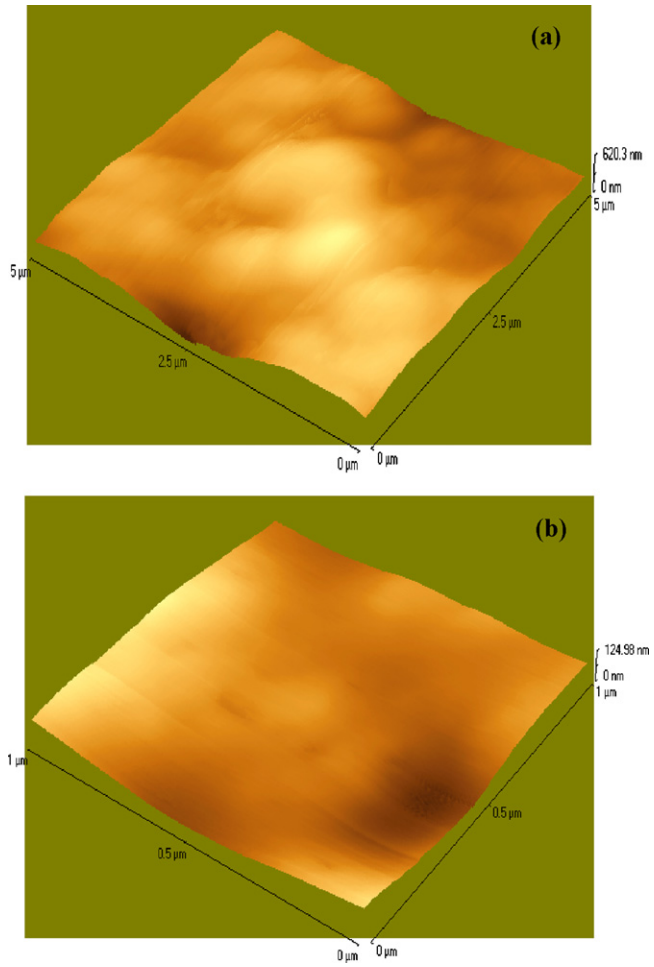

Fig. 3. AFM images of polymer gel electrolyte films containing: (a) 3 wt.% MgO and (b) 10 wt.% MgO.

MgO, observed at 38.6 and 44.4°, along with some PVdF-HFP peaks (Fig. 1c). This confirms the composite nature of the film.

The morphology of the undispersed gel polymer electrolyte and gel nanocomposite polymer electrolyte (with 10 wt.% MgO) film was examined by SEM and the images are shown in Fig. 2. The undispersed gel polymer electrolyte film is seen to have uniform small pores at the microscopic level (Fig. 2a). In the gel polymer electrolyte nanocomposite film, a uniform dispersion of nanosized MgO particles is observed whereas the pores are indistinct (Fig. 2b). To examine further the surface morphology at the microscopic level, AFM images were recorded on the surface of a nanocomposite polymer electrolyte film and are presented in Fig. 3. The surface is almost flat and uniform without pores or any phase separation, which is indicative of the high affinity of the polymer host, PVdF-HFP with the liquid electrolyte.

In order to investigate ion-polymer interaction and possible conformational changes in the host polymer due to the Mg-salt

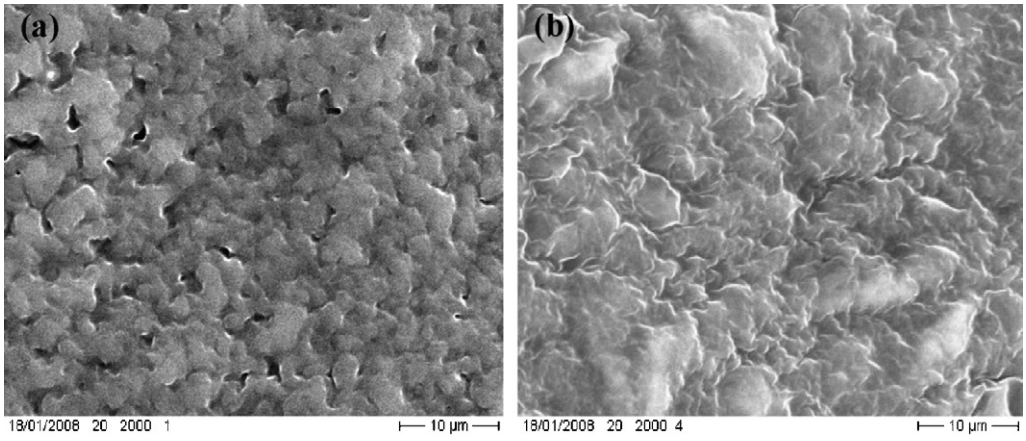

Fig. 2. SEM images of gel polymer electrolyte films containing (a) 0 wt.% MgO, and (b) 10 wt.% MgO.

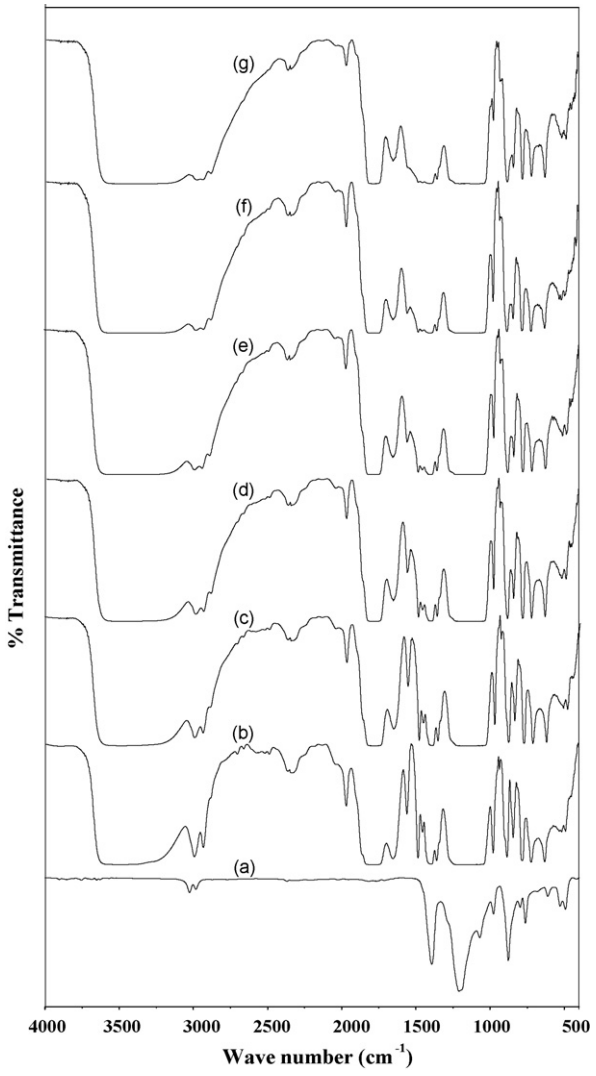

Fig. 4. FTIR spectra of (a) PVdF-HFP (pure) film and gel polymer electrolyte films containing MgO nanoparticles of: (b) 0 wt.%, (c) 3 wt.%, (d) 7 wt.%, (e) 10 wt.%, (f) 15 wt.% and (g) 20 wt.%.

containing liquid electrolyte entrapment and dispersion of MgO nanoparticles, FTIR spectroscopic analysis was conducted. The comparative FTIR spectra of the host polymer PVdF-HFP and the gel polymer electrolyte films with different MgO content (0–20 wt.%) are given in Fig. 4. The following distinctive features have been extracted from this spectral response.

(i) The conformational changes in the semi-crystalline host polymer PVdF-HFP due to the addition of liquid electrolyte were monitored. Peaks corresponding to the bands at 484, 528 (very weak), 762, 839, 879 and 976 cm^{-1} are observed and assigned in Table 1. The peaks at 528 and 976 cm^{-1} are due to a non-polar *trans-gauche-trans-gauche′* (TGTG′) conformation (i.e., an α-phase) of the semi-crystalline PVdF-HFP [28–30]. The peak at 484 cm^{-1} is due to an intermediate polar TTTGTTTG' conformation (γ-phase), which occurs when the polymer is moderately stressed [31]. Other bands are very weak and/or overlap the band associated with the EC–PC or Mg-salt. It may be noted that the band at 762 cm^{-1} (assigned to the α-phase) disappears due to the addition of liquid electrolyte. Further, the bands at 839 and 879 cm^{-1}, assigned to the amorphous phase, appear as a symmetrical peak. The band at 879 cm^{-1} becomes sufficiently broad, and appears to be the sum of two peaks. These observations indicate the substantial conformational changes in the crystalline texture of the host polymer PVdF-HFP due to the interaction with liquid electrolyte. The disappearance of some bands associated with the crystalline α-phase and the appearance of the bands of the amorphous phase of the polymer indicate the reduction of crystallinity and dominance of the amorphous phase in the gel nanocomposite polymer electrolyte.

Table 1
Assignment of important FTIR bands of PVdF-HFP and perchlorate anion $(ClO_4)^-$.

	IR bands (cm^{-1})	Assignment
PVdF-HFP	484	γ-Phase
	528 (very weak)	
	762	α-Phase
	976	
	839	Amorphous phase
	879	
$(ClO_4)^-$	623	ν_4 $(ClO_4)^-$
	628	Ion pairs/aggregates

(ii) The stretching vibration (ν_4) mode of the ClO_4^- anion observed in the range of 650–600 cm^{-1} has been probed to obtain the information on the degree of salt dissociation in the gel polymer electrolyte. The expanded portion of the spectra in the range 650–600 cm^{-1} is shown in Fig. 5. The peaks at ~628 and

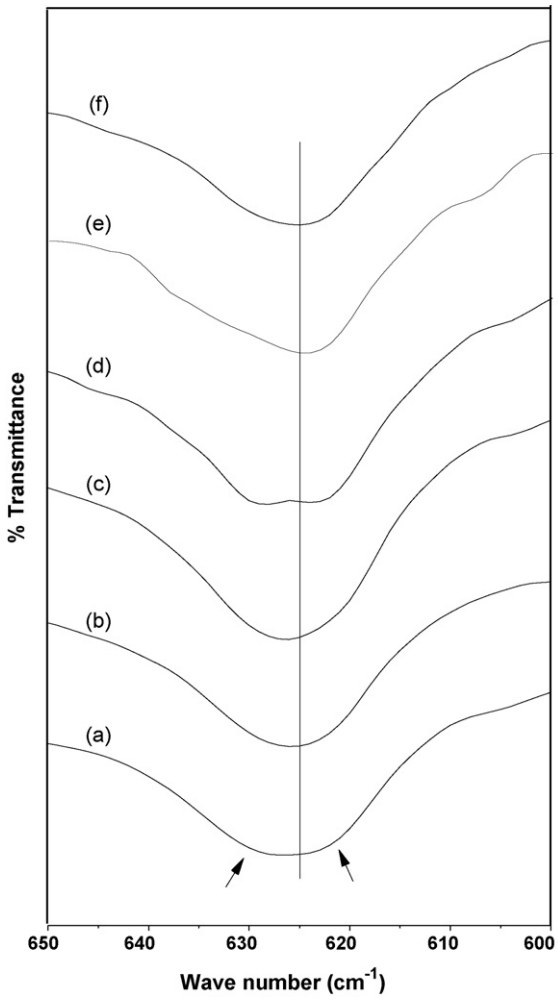

Fig. 5. Expanded representation of FTIR spectra of gel composite polymer electrolyte films containing MgO nanoparticles of: (a) 0 wt.%, (b) 3 wt.%, (c) 7 wt.%, (d) 10 wt.%, (e) 15 wt.% and (f) 20 wt.% in 600–650 cm^{-1} region.

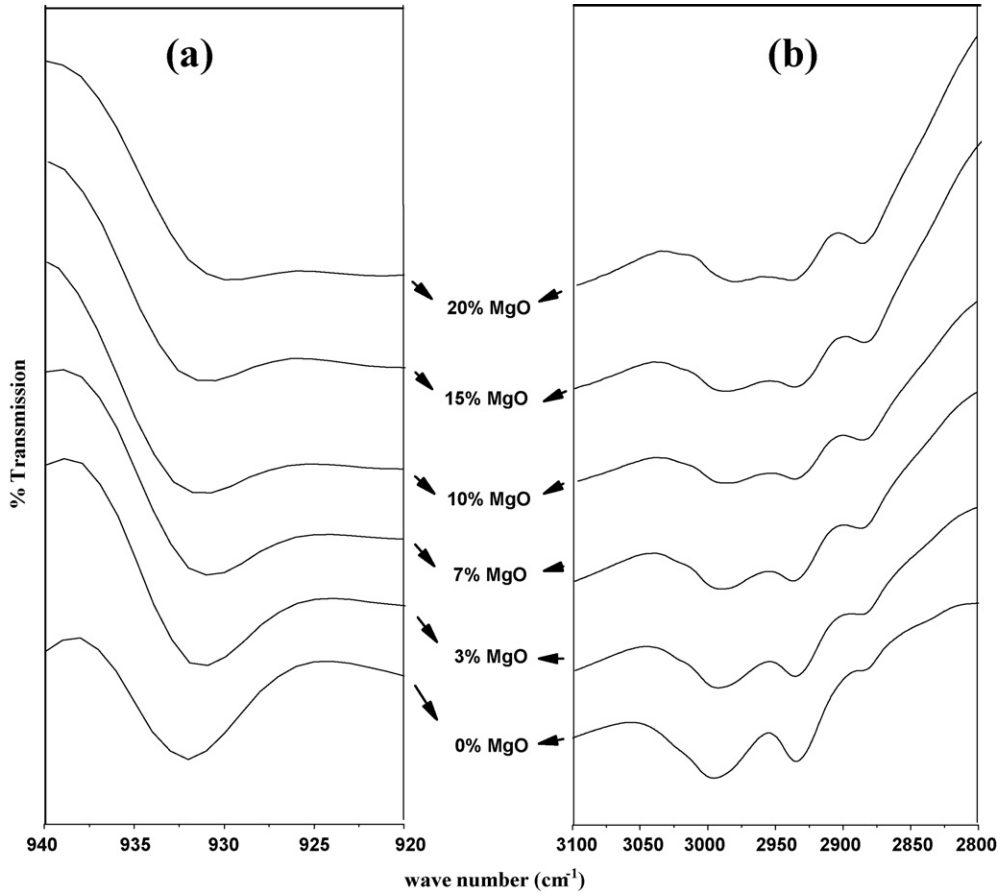

Fig. 6. Expanded representation of FTIR spectra of gel polymer electrolyte films containing different amounts of MgO nanoparticles for spectral regions: (a) 920–940 cm^{-1} and (b) 2800–3100 cm^{-1}.

~623 cm^{-1} are attributed to the ion-pair and the free $(ClO_4)^-$, respectively [32]. In the undispersed gel polymer electrolyte, the peak at ~626 cm^{-1} appears to be the sum of two nearby peaks associated with the free and paired $(ClO_4)^-$ ions (Fig. 5a). The dispersion of MgO nanoparticles in the gel polymer electrolyte influences this band; the peak becomes broader and the two peaks appear well separated (Fig. 5). This is associated with the filler–anion interaction in the gel polymer electrolyte nanocomposite.

(iii) The dispersion of MgO nanoparticles in the gel polymer electrolyte also affects the ring stretching and breathing mode of PC at ~932 cm^{-1}(expanded portion shown in Fig. 6a) [33]. This band shifts downward with increasing MgO content. The intensity of the broad bands between 2850 and 3050 cm^{-1} (the –CH– stretching mode of the main polymer chain) changes substantially due to the MgO dispersion. The shifts in these bands are distinctly observed (Fig. 6b). These changes indicate a substantial modification in the lattice environment, that has a significant influence on ion conduction in the gel polymer system.

3.2. Thermal studies

The DSC thermograms of pure PVdF-HFP, filler-free gel polymer electrolyte and gel nanocomposites are shown in Fig. 7a–g. The glass transition temperature (T_g) is observed at −65 °C for pure PVdF-HFP film. After the gel formation due to the addition of liquid electrolyte in host polymer, the T_g values generally decrease, possibly below −90 °C in the present case, which is not observable due to the limitation of equipment. A step change is observed between 0 and 5 °C due to the dispersion of nanosized MgO in nanocomposite gels (Fig. 7d–g). This step change is possibly attributed to the glass transition temperature of a separate nanocomposite phase formed through interaction of MgO nanoparticles with the gel polymer electrolyte. This step change is not clearly observed for lower contents of filler, MgO nanoparticles (Fig. 7b and c). Further, no endothermic peak is found and the electrolyte film remains stable in the same gel phase over a substantially wide temperature range from −70 to 80 °C, which is advantageous for potential applications in electrochemical devices.

TGA curves of pure PVdF-HFP, undispersed gel polymer electrolyte and gel nanocomposite dispersed with 10 wt.% MgO are shown in Fig. 8. As observed from Fig. 8a, the host polymer PVdF-HFP is highly thermally stable as almost no weight loss occurs up to ~400 °C. A marginal weight loss (~5 wt.%) has been observed up to ~90 °C for both the undispersed and dispersed gel polymer electrolytes, which may be due to surface adsorbed moisture. Thereafter, a substantial weight loss occurs due to the evaporation of the EC and PC solvents. A slightly better retentivity for EC and PC has been observed due to the addition of MgO nanoparticles in the nanocomposites, as shown in Fig. 8c.

3.3. Electrical properties

3.3.1. Electrical conductivity

The variation of room-temperature electrical conductivity of gel polymer electrolyte nanocomposites with respect to the content of dispersed MgO nanoparticles is given in Fig. 9. The addition of MgO particles results an initial increase in the conductivity followed by two maxima observed at ~3 and ~10 wt.% MgO (Fig. 9). Such

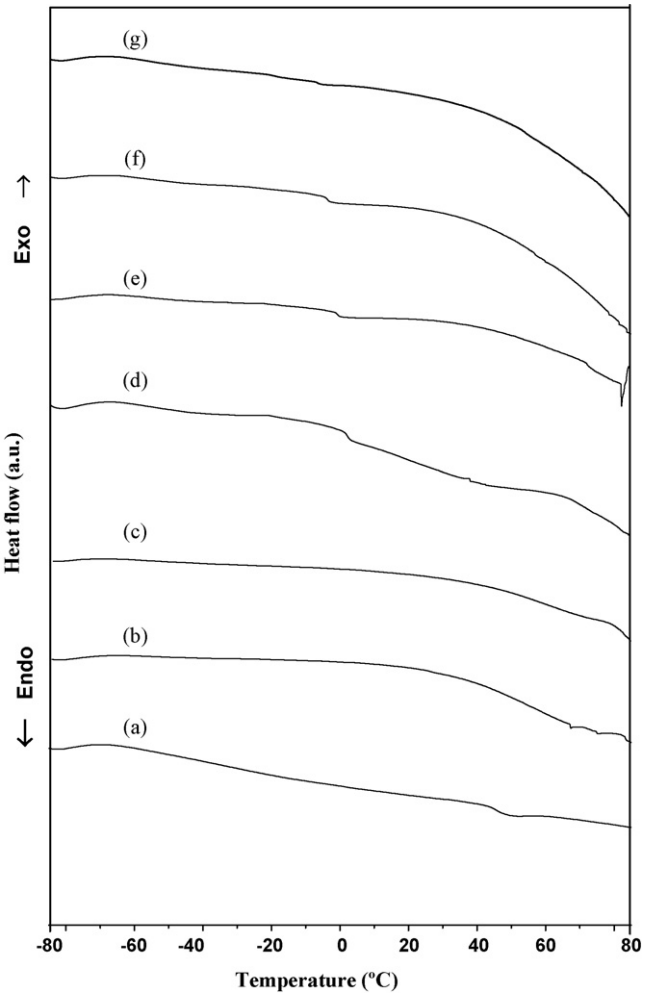

Fig. 7. DSC curves of gel polymer electrolyte films: (a) PVdF-HFP (pure) film and gel polymer electrolyte films containing (b) 0 wt.%, (c) 7 wt.%, (d) 10 wt.%, (e) 12 wt.%, (f) 15 wt.% and (g) 20 wt.% MgO nanoparticles.

two maxima have recently been reported for an ion-conducting gel polymer electrolyte composite [34] and solvent-free composite polymer electrolytes [35–37]. The first conductivity maximum is possibly due to the dissociation of ion aggregates/undissociated

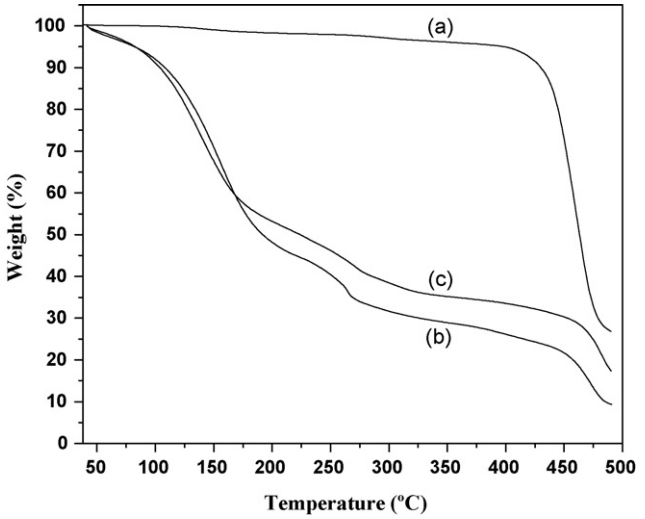

Fig. 8. TGA curve of (a) pure PVdF-HFP film and gel polymer electrolyte films containing: (b) 0 wt.% and (c) 10 wt.% MgO nanoparticles.

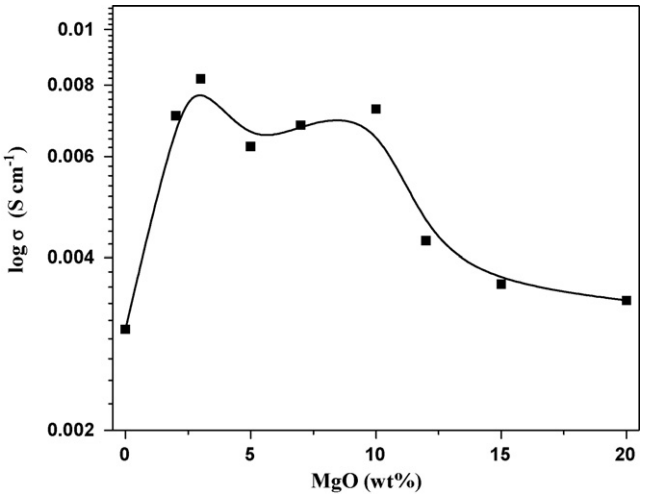

Fig. 9. Room-temperature conductivity of gel composite polymer electrolyte films as function of nanosized MgO content.

salt into free ions with the addition of nanosized MgO particles, whereas the second conductivity maximum is related to the composite effect and explained on the basis of the formation of a conducting interfacial space-charge double-layer between the nanosized MgO particles and polymer gel electrolytes [38,39]. The decrease in conductivity after the second conductivity maximum is generally related to the blocking effect of filler particles, which hinders the motion of mobile ions [40]. The optimum conductivity value at room temperature (~25 °C) of the gel nanocomposite is $\sim 8 \times 10^{-3}\,S\,cm^{-1}$ at 3 wt.% MgO. An approximate three-fold enhancement in ionic conductivity is observed on dispersion of MgO nanoparticles in the gel polymer electrolytes along with a substantial improvement in their mechanical strength.

Fig. 10 shows the temperature dependence of the conductivity of gel polymer electrolyte nanocomposite films. The 'σ vs. $1/T$' curves for gel nanocomposites are linear up to ~60 °C, thereafter no conductivity enhancement is observed. The linear relationship suggests an Arrhenius-type thermally activated process following the expression:

$$\sigma = \sigma_0 \exp\left(\frac{-E_a}{kT}\right) \quad (2)$$

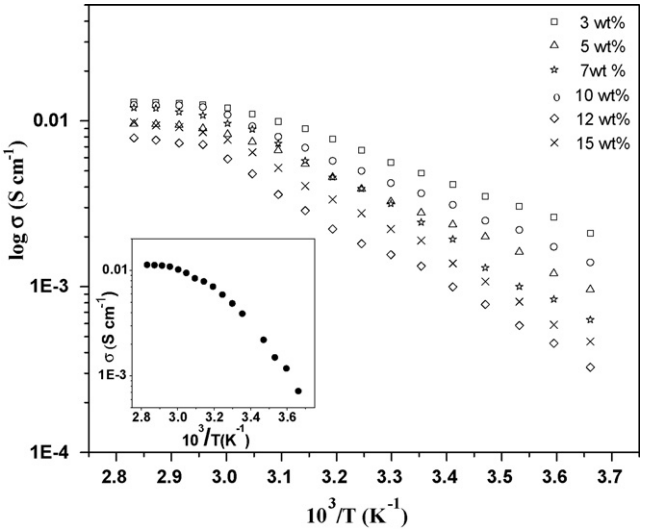

Fig. 10. 'σ vs. $1/T$' plots of gel polymer electrolyte nanocomposite films. 'σ vs. $1/T$' plot of filler-free gel polymer electrolyte is shown in inset.

Table 2
Different parameters (σ_0 and E_a) for gel polymer electrolyte nanocomposites obtained by linear fitting of conductivity to Arrhenius equation.

MgO content in gel polymer electrolyte (wt.%)	σ_0 (S cm^{-1})	E_a (eV)
3	4.59×10^1	0.235
5	4.64×10^1	0.237
7	6.82×10^3	0.383
10	6.6×10^1	0.252
12	2.43×10^3	0.364
15	1.02×10^3	0.350

where E_a is activation energy, σ_0 is a pre-exponential factor, and k is the Boltzmann constant. These parameters have been evaluated and are listed in Table 2. The temperature dependence of the filler-free gel polymer electrolyte shows non-linear behaviour (inset of Fig. 9), and follows the Vogel–Tammen–Fulcher (VTF) equation:

$$\sigma = AT^{-1/2} \exp\left(\frac{-B}{T - T_0}\right) \quad (3)$$

where the parameter B is associated with the rate at which viscosity changes with temperature, A is a pre-exponential factor, i.e., the conductivity at infinitely high temperature, and T_0 is the equilibrium glass transition temperature close to the T_g values. These parameters have been evaluated and found to be: $B = 0.46$ eV, $A = 1.21$ S cm^{-1} K$^{1/2}$ and $T_0 = 179$ K. From the temperature-dependent electrical conductivity measurements, it may be noted that the optimized Mg^{2+} gel polymer electrolyte nanocomposite (i.e., with 3 wt.% MgO content) exhibits ionic conductivity of the order of $\sim 2 \times 10^{-3}$ S cm^{-1} at 0 °C and 1×10^{-2} S cm^{-1} at 80 °C, showing promise for potential application in Mg-batteries over a substantially wider temperature range.

3.3.2. Transport number

The total ionic (cationic and anionic) transport number (t_{ion}) has been evaluated using polarization method, as described in Section 2. Fig. 11 shows the variation of polarizing current through a typical cell: SS|gel nanocomposite with 10 wt.% MgO|SS as a function of time on applying a voltage of 1.0 V. The value of t_{ion} is determined using Eq. (1) and found to be >0.99 for all the gel films. This shows that the overall conductivity of the pure gel electrolyte and its nanocomposites is predominantly ionic. No electronic conductivity is expected in the gel-like electrolytes where liquid electrolytes are entrapped in the almost inert network of polymer hosts and liquid-like charge transport takes place in such systems.

The cationic transport number at room temperature is a key parameter to evaluate the performance of the electrolytes. In the present case, the transport number (t_+) of Mg^{2+} ions in the gel electrolyte films is obtained from a combination of AC and DC techniques, as proposed by Evans et al. [27]. In this technique, the Mg|gel nanocomposites|Mg cells were polarized potentiostatically by applying a voltage, $\Delta V = 0.3$ V for 3–4 h and subsequently the initial and final currents were recorded. As a part of the technique, the cells were subjected to AC impedance measurements prior to and after the polarization. Values of the electrode–electrolyte contact resistances were obtained from the impedance plots. The t_+ values were calculated using the expression:

$$t_+ = \frac{I_s(\Delta V - R_o I_o)}{I_o(\Delta V - R_s I_s)} \quad (4)$$

where I_o and I_s are the initial and final currents; R_o and R_s are the cell resistances before and after the polarization. A typical DC polarization current vs. time plot and AC impedance plots are shown in Fig. 12a and b. The values of t_+ at room temperature, evaluated for gel polymer electrolyte films with different values of nanosized MgO content, are listed in Table 3. The Mg^{2+} ion transport num-

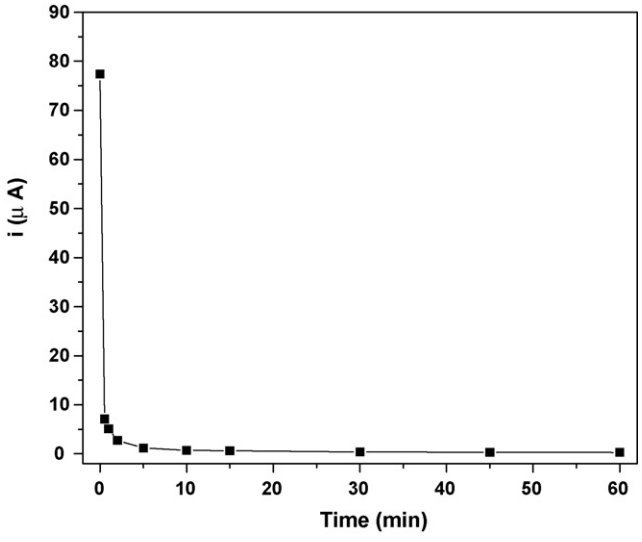

Fig. 11. DC polarization curve of symmetric SS|gel nanocomposite with 10 wt.% MgO|SS cell at room temperature on applying a voltage of 1.0 V.

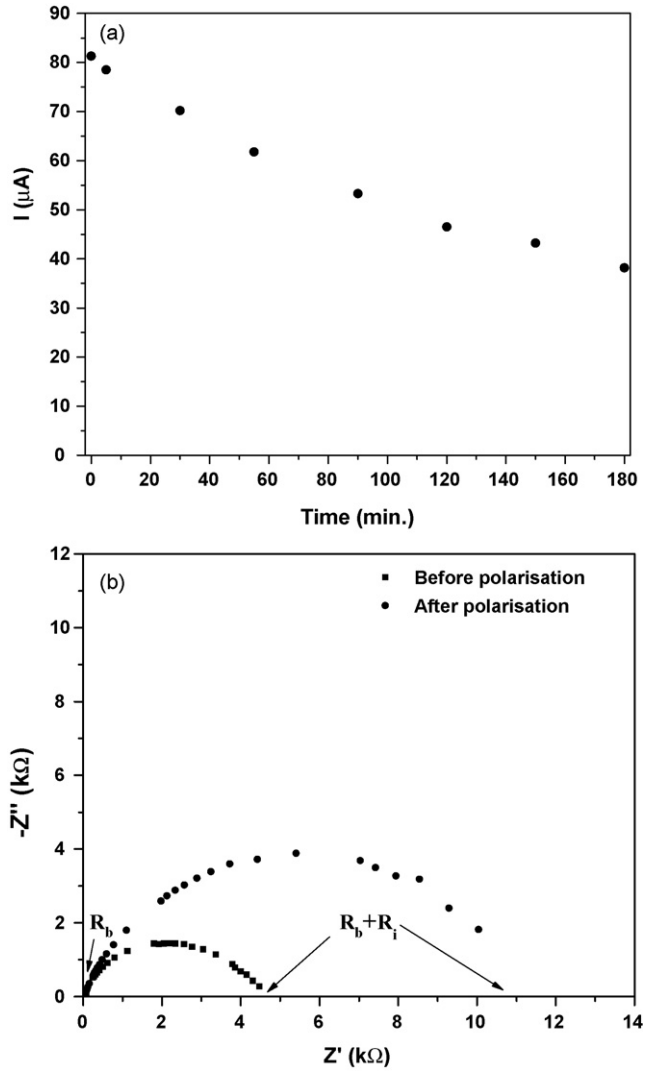

Fig. 12. (a) DC polarization curve of a typical symmetric Mg|gel nanocomposite with 10 wt.% MgO|Mg cell at room temperature, and (b) AC complex impedance plot before and after DC polarization of cell.

ber increases substantially with increase in the amount of MgO nanoparticles up to a maximum value of $t_+ = 0.44$ for 10 wt.% dispersion. Thereafter, the t_+ value slightly decreases due to the further addition of MgO particles to the gel electrolyte system.

The enhancement in cationic transport number with addition of nanosized inorganic fillers in the PEO-based composite polymer electrolytes has been reported [41–43]. Scrosati et al. [42,43] explained this behaviour in terms of the Lewis acid–base reaction between the ceramic surface states and the PEO segments based on the theory proposed by Wieczorek et al. [44,45]. Accordingly, ceramic fillers promote surface conducting pathways due to Lewis acid–base type interaction with PEO segments, through which ions (Li^+ ions) move freely and hence enhancement of the cationic transference number is observed. Further, Kumar et al. [39,40] has explained systematically the transport mechanism in the colloidal phase of liquid and polymer electrolytes on the basis of space-charge double-layer formation between ceramic particles and polymer electrolyte surface based on the theory originally proposed by Maier [38] for the ionic conduction in solid composites. Accordingly, the space-charge regions formed due to the addition of ceramic particles in gel electrolytes are localized sources of electric fields, which influence the movement of charged species. Due to the introduction of ceramic fillers in the gel-like electrolytes, the cations may either be transported through the liquid phase of the gel polymer electrolyte or through the double-layer formed due to the ceramic fillers. The space-charge regions (double-layers) facilitate the ionic motion and hence transport number enhancement is observed. This enhancement effect is observed up to a certain volume fraction of the space-charge region. As the volume fraction increases beyond a certain point, space-charge regions start giving a blocking effect that leads to a possible lowering of the transport number [40].

The materials in the present study, in which MgO nanoparticles are dispersed in Mg^{2+} ion-conducting gel polymer electrolytes, are almost similar to those examined by Kumar et al. [39,40]. The MgO nanoparticles are slightly electronegative in nature and hence there is a possibility of the following reversible reaction when these fillers are dispersed in the gel electrolyte system:

$$MgO + Mg^{2+} \rightleftharpoons MgO : Mg^{2+} \quad (5)$$

The MgO:Mg^{2+} species form space-charge regions and induce a local electric field. This local field is possibly responsible for the enhanced Mg^{2+} ion motion and hence enhanced transport number up to the addition of certain extent of filler amount, e.g., ~10 wt.% MgO. The decrease in the transport number (Table 3) is explained on the basis of the blocking effect of the space-charge region due to the further addition of MgO nanoparticles [40].

3.4. Electrochemical properties

In order to confirm Mg^{2+} ion conduction in the gel polymer electrolyte nanocomposite films, complex impedance spectroscopy and cyclic voltammetric studies were performed on symmetrical SS|gel nanocomposite|SS (Cell-I) and Mg|gel nanocomposite|Mg (Cell-II). In Cell-I, the gel film was in contact with a stainless steel (SS), a blocking electrode, whereas foils of Mg were used as reversible electrodes in Cell-II. Fig. 13 gives the comparative complex impedance plots for Cell-I and Cell-II recorded at room temperature (~25 °C). The impedance response of Cell-I (with SS electrodes) shows the steep rising behaviour of an imaginary impedance in the low-frequency range, indicating the ion blocking nature of the SS electrodes (Fig. 13a). On the other hand, almost well-defined semicircular dispersion curve is observed for Cell-II (with Mg electrodes), as shown in Fig. 13b. The appearance of a well-defined semi-circle for the Mg|gel nanocomposite|Mg cell clearly indicates that the Mg metal attains equilibrium with the Mg^{2+} ions in the gel polymer electrolyte nanocomposite. Such behaviour has recently been reported for a Li|gel electrolyte|Li cell [46]. The bulk resistance of the gel film (R_b) was obtained from the high-frequency intercept of the complex plane plots and the interfacial resistance (R_i) was calculated from the low-frequency intercept. The values of R_b measured for both the cells are almost in the same range (~15–40 Ω cm^2) (Fig. 13, inset). The value of R_i for the Mg/gel nanocomposite is ~7 kΩ cm^2, whereas for the SS/gel nanocomposite it is ~100 kΩ cm^2. The substantially lower value of R_i for the Mg/gel nanocomposite interface further demonstrates that equilibrium has been established between Mg metal and Mg^{2+} ions. These observations further confirm Mg^{2+} ion conduction in the gel polymer electrolyte nanocomposite.

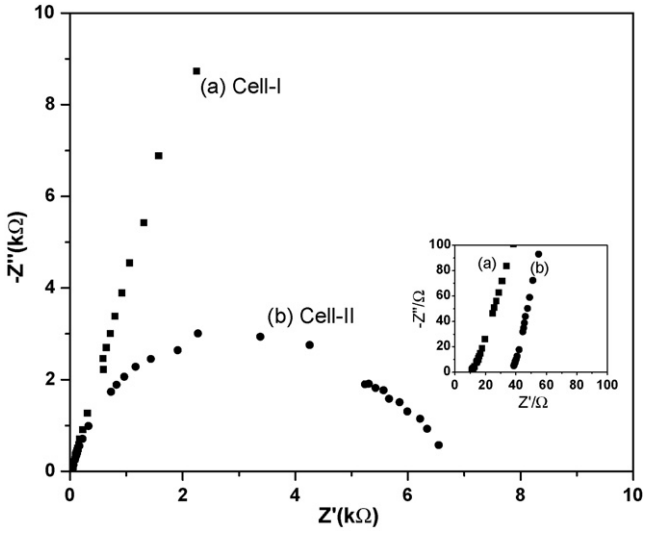

Fig. 13. Complex impedance plots for (a) Cell-I: SS|gel nanocomposite|SS, and (b) Cell-II: Mg|gel nanocomposite|Mg recorded at room temperature. High-frequency region is expanded and shown in inset.

Fig. 14 shows cyclic voltammograms (CVs) for cells containing gel electrolyte films with different amounts of MgO nanoparticles sandwiched between two symmetrical Mg electrodes at a scan rate of 5 mV s^{-1}. The CV for the cell with symmetrical SS electrodes is also shown for comparison. The cathodic and anodic current peaks are distinctly observed for the cells with Mg electrodes, whereas no such features are present in the case of the cell with SS electrodes in the same potential range (Fig. 14). This suggests the following reversible reaction:

$$Mg^{2+} + 2e^- \rightleftharpoons Mg^0 \quad (6)$$

i.e., the cathodic deposition and anodic oxidation of Mg are facile at the Mg|gel electrolyte interface. This it is the indicative of Mg^{2+} ion conduction in the gel polymer electrolyte nanocomposite films. It may be noted that the cathodic/anodic peak potentials are separated by several volts, similar to the other cases, e.g., the Li|PEO + $LiBF_4$ film|Li cell reported by Munichandraiah et al. [47]. This is possible because the experiments were carried out on cells

Table 3
Mg^{2+} ion transport number of gel polymer electrolyte containing different amount of MgO nanoparticles.

MgO (in wt.%)	Mg^{2+} ion transport number
0	0.22 ± 0.02
3	0.30 ± 0.02
5	0.36 ± 0.02
10	0.44 ± 0.02
15	0.33 ± 0.02

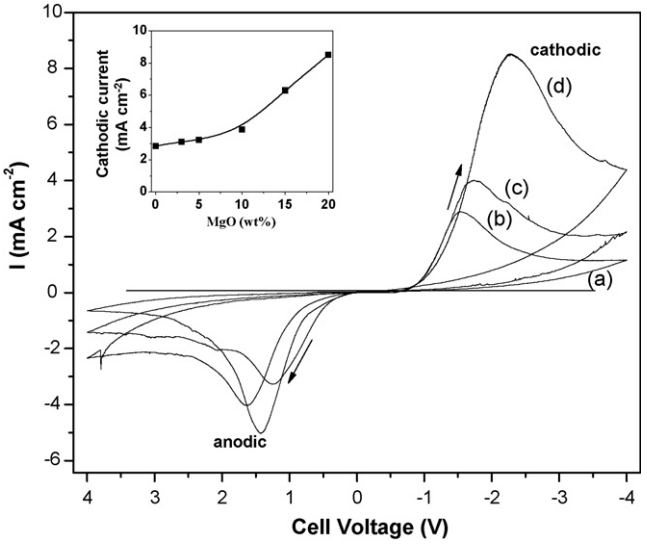

Fig. 14. Cyclic voltammograms of cells: SS|gel nanocomposite|SS (a), and Mg|gel nanocomposite|Mg with MgO content of 0 wt.% (b), 10 wt.% (c) and 20 wt.% (d), recorded at room temperature at scan rate of 5 mV s^{-1}. Variation of cathodic current as function of MgO content is shown in inset.

with two electrode geometry without using a reference electrode. A substantial increase in the amount of anodic and cathodic peak currents has also been observed due to the addition of nanosized MgO particles in the gel polymer electrolyte, as shown in Fig. 14 (inset). This observation supports the role of active filler MgO nanoparticles dispersed in gel electrolyte for the reversible reaction (5) and the formation of space-charge regions (double-layers), responsible for enhanced Mg^{2+} ion conduction.

The electrochemical stability of the gel films has also been tested using linear sweep voltammetry (LSV) recorded on a SS|gel nanocomposite|Mg cell. As seen in Fig. 15, the electrolyte films are stable up to ~3.5 V. The stability is slightly enhanced due to the addition of nanosized MgO particles. This value of working voltage range (i.e., electrochemical potential window) appears to be high enough to use the gel polymer electrolyte nanocomposite films as a solid-state-like separator/electrolyte in Mg-batteries and supercapacitors.

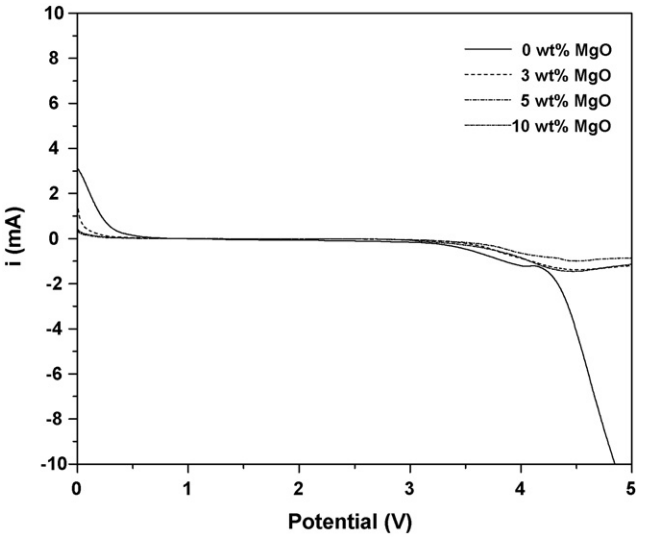

Fig. 15. Linear sweep voltammograms of SS|gel nanocomposites|Mg cells with different MgO contents at scan rate of 5 mV s^{-1}.

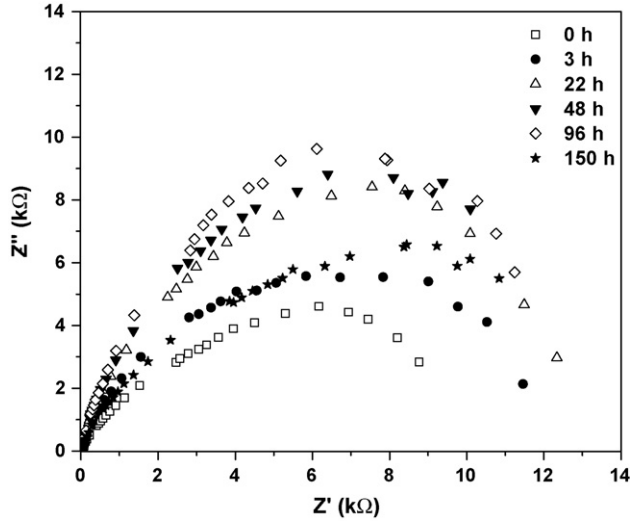

Fig. 16. Complex impedance spectra of Mg|gel nanocomposite with 10 wt.% MgO|Mg cell at different intervals of ageing at room temperature.

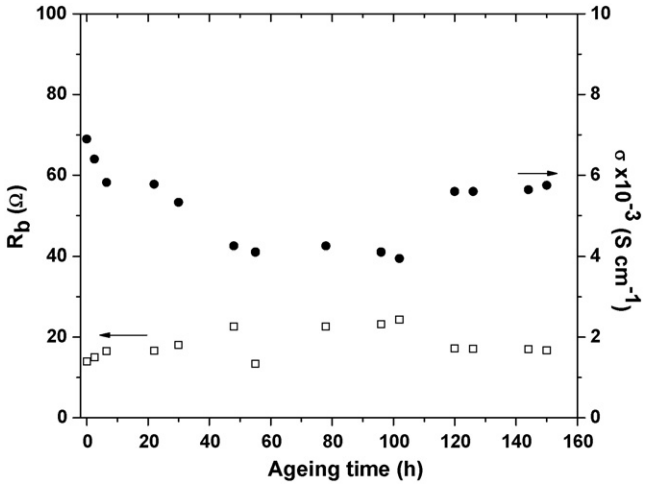

Fig. 17. Variation of (a) bulk resistance and (b) conductivity of Mg|gel nanocomposite with 10 wt.% MgO|Mg cell with ageing time.

The electrode|electrolyte interfacial stability is an important aspect to evaluate over a long duration from a battery application point of view. For this purpose, a typical symmetrical Mg|gel nanocomposite with 10% MgO|Mg cell was assembled and its AC impedance spectra were recorded at different time intervals, as shown in Fig. 16. The size of the semicircle increases with time, as observed in Fig. 16. Such behaviour has also been observed for a lithium system (i.e., Li/gel electrolyte interface) [46]. An almost stable value of the bulk resistance R_b (between 14 and 23 Ω) persists for about 100 h (Fig. 17). The overall conductivity, σ, is also found to be almost constant (4×10^{-3} S cm^{-1}) for quite long time (Fig. 16b). This indicates that there is no loss of solvent (EC + PC) from the gel on ageing. The charge-transfer resistance (R_{ct}) increases initially then becomes constant at around 12 kΩ. This result can possibly be attributed to better interfacial stability due to the incorporation of nanosized MgO particles in the gel polymer electrolyte.

4. Conclusions

The present work reports the characterization of a PVdF-HFP based Mg^{2+} ion-conducting gel polymer electrolyte nanocomposites dispersed with nanosized MgO particles. The results confirm

that the addition of nanosized MgO is beneficial in inducing consistent improvements in liquid electrolyte retention as well as in the overall chemical, physical and electrochemical properties. On the basis of various structural, thermal, electrical and electrochemical studies, the following conclusions can be drawn.

(i) The composite nature of the gel electrolyte films due to dispersion of MgO nanoparticles is confirmed from XRD and SEM results.
(ii) Substantial conformational changes in the crystalline texture of the host polymer PVdF-HFP are observed due to immobilization of the liquid electrolyte in the gel polymer electrolyte. The existence of free anion and filler–polymer interaction is confirmed from FTIR studies.
(iii) The nanocomposite offers high ionic conductivity ($\sigma \sim 10^{-3}\,S\,cm^{-1}$ at room temperature) with a wider electrochemical potential window and good thermal stability having single-phase behaviour over a temperature range from −70 to 80 °C.
(iv) Studies based on AC impedance spectroscopy and cyclic voltammetry indicate the existence of an electrochemical equilibrium between Mg metal and Mg^{2+} ions and hence confirm Mg^{2+} ion conduction in the gel nanocomposite polymer electrolyte.
(v) The Mg^{2+} ion transport number is almost doubled due to the addition of 10 wt.% MgO nanoparticles. The enhancement is explained on the basis of the formation of space-charge (double-layer) regions due to the presence of MgO:Mg^{2+}-like species, which support Mg^{2+} ion motion.
(vi) The optimized gel polymer electrolyte nanocomposite appears to be an excellent substitute for the liquid electrolyte in electrochemical devices, particularly in rechargeable magnesium batteries.

Acknowledgements

Authors acknowledge the financial supports received from the Council of Scientific & Industrial Research, New Delhi (Sanction No.: 03(1069)/06/EMR-II, 2006) and University of Delhi (under the Scheme to strengthen R&D Doctoral Research Programme providing funds to University faculty, 11-17 Research Fund, 2008). One of the authors (GPP) thanks the Council of Scientific & Industrial Research, New Delhi for the award of Senior Research Fellowship. The authors are grateful to Prof. Binod Kumar, University of Dayton Research Institute, Dayton, USA, for his informative comments on the work.

References

[1] J.R. MacCallum, C.A. Vincent, Polymer Electrolyte Reviews-I & II, Elsevier, London, 1987 and 1989.
[2] F.M. Gray, Solid Polymer Electrolytes—Fundamentals and Technological Applications, VCH, New York, 1991;
F.M. Gray, Polymer Electrolytes, Royal Society of Chemistry Monographs, Cambridge, 1997.
[3] R.C. Agrawal, G.P. Pandey, J. Phys. D: Appl. Phys. 41 (2008) 223001.
[4] J.-M. Tarascon, M. Armand, Nature 414 (2001) 359–367.
[5] P. Novak, R. Imhof, O. Hass, Electrochim. Acta 45 (1999) 351–367.
[6] D. Aurbach, Y. Gofer, Z. Lu, A. Schechter, O. Chusid, H. Gizbar, Y. Cohen, V. Ashkenazi, M. Moshkovich, R. Turgeman, E. Levi, J. Power Sources 97–98 (2001) 28–32.
[7] D. Aurbach, G.S. Suresh, E. Levi, A. Mitelman, O. Mizrahi, O. Chusid, M. Brunelli, Adv. Mater. 19 (2007) 4260–4267.
[8] D. Aurbach, Z. Lu, A. Schechter, Y. Gofer, H. Gizbar, R. Turgeman, Y. Cohen, M. Moshkovich, E. Levi, Nature 407 (2000) 724–727.
[9] E. Lancry, E. Levi, Y. Gofer, M. Levi, G. Salitra, D. Aurbach, Chem. Mater. 16 (2004) 2832–2838.
[10] E. Levi, M.D. Levi, O. Chusid, D. Aurbach, J. Electroceram., in press.
[11] Z. Lu, A. Schechter, M. Moshlovich, D. Aurbach, J. Electroanal. Chem. 466 (1999) 203–217.
[12] J.Y. Song, Y.Y. Wang, C.C. Wan, J. Power Sources 77 (1999) 183–197.
[13] S.A. Hashmi, Natl. Acad. Sci. Lett. 27 (2004) 27–46.
[14] N. Yoshimoto, Y. Tomonaga, M. Ishikawa, M. Morita, Electrochim. Acta 46 (2001) 1195–1200.
[15] G.G. Kumar, N. Munichandraiah, J. Electroanal. Chem. 495 (2000) 42–50.
[16] D.K. Rai, S.A. Hashmi, Y. Kumar, G.P. Pandey, in: S.A. Hashmi, Amita Chandra, Amreesh Chandra (Eds.), Electroactive Polymers: Materials and Devices, vol. II, Allied Publishers, New Delhi, 2007, pp. 407–411.
[17] G.G. Kumar, N. Munichandraiah, J. Power Sources 102 (2001) 46–54.
[18] M. Morita, N. Yoshimoto, S. Yakushiji, M. Ishikawa, Electrochem. Solid-State Lett. 4 (2001) A177–A179.
[19] S.H. Chung, Y. Wang, L. Persi, F. Croce, S.G. Greenbaum, B. Scrosati, E. Plichta, J. Power Sources 97–98 (2001) 644–648.
[20] M. Forsyth, D.R. MacFarlane, A. Best, J. Adebahr, P. Jacobsson, A.J. Hill, Solid State Ionics 147 (2002) 203–211.
[21] A.M. Stephan, K.H. Nahm, Polymer 47 (2006) 5952–5964.
[22] J.-M. Tarascon, A.S. Gozdz, C.N. Schmutz, F.K. Shokoohi, P.C. Warren, Solid State Ionics 86–88 (1996) 49–54.
[23] G.B. Appetecchi, P. Romagnoli, B. Scrosati, Electrochem. Commun. 3 (2001) 281–284.
[24] N. Byrne, J. Efthimiadis, D.R. MacFarlane, M. Forsyth, J. Mater. Chem. 14 (2004) 127–133.
[25] V. Gentili, S. Panero, P. Reale, B. Scrosati, J. Power Sources 170 (2007) 185–190.
[26] S.A. Hashmi, S. Chandra, J. Mater. Sci. Eng. B 34 (1995) 18–26.
[27] J. Evans, C.A. Vincent, P.G. Bruce, Polymer 28 (1987) 2324–2328.
[28] R. Gregorio Jr., M. Cestari, J. Polym. Sci. B 32 (1994) 859–870.
[29] S. Abbrent, J. Plestil, D. Hlavata, J. Lindgren, J. Tegenfeldt, A. Wendsjo, Polymer 42 (2001) 1407–1416.
[30] A. Martinelli, A. Matic, P. Jacobsson, L. Börjesson, M.A. Navarra, S. Panero, B. Scrosati, J. Electrochem. Soc. 154 (2007) G183–G187.
[31] S.K. Tripathy, R. Potenzone Jr., A.J. Hopfinger, N.C. Banik, P.L. Taylor, Macromolecules 12 (1979) 656–658.
[32] H.W. Chen, C.Y. Chiu, F.C. Chang, J. Polym. Sci. Part B Polym. Phys. 40 (2002) 1342–1353.
[33] D. Battisti, G.A. Nazri, B. Klassen, R. Aroca, J. Phys. Chem. 97 (1993) 5826–5830.
[34] J.P. Sharma, S.S. Sekhon, Solid State Ionics 178 (2007) 439–445.
[35] B.K. Choi, K. Shin, Solid State Ionics 86–88 (1996) 303–306.
[36] S.A. Hashmi, H.M. Upadhayaya, A.K. Thakur, in: B.V.R. Chowdari, Wenji Wang (Eds.), Solid State Ionics: Materials and Devices, World Scientific, Singapore, 2000, p. 461.
[37] G.P. Pandey, S.A. Hashmi, R.C. Agrawal, Solid State Ionics 179 (2008) 543–549.
[38] J. Maier, Solid State Ionics 70–71 (1994) 43–51;
J. Maier, Prog. Solid State Chem. 23 (1995) 171–263.
[39] B. Kumar, J. Power Sources 135 (2004) 215–231.
[40] B. Kumar, S. Nellutla, J.S. Thokchom, C. Chen, J. Power Sources 160 (2006) 1329–1335.
[41] C. Capiglia, P. Mustarelli, E. Quartarone, C. Tomasi, A. Magistris, Solid State Ionics 118 (1999) 73–79.
[42] F. Croce, R. Curini, A. Martinelli, L. Persi, F. Ronci, B. Scrosati, J. Phys. Chem. B 103 (1999) 10632–10638.
[43] B. Scrosati, F. Croce, S. Panero, J. Power Sources 100 (2001) 93–100.
[44] W. Wieczorek, Z. Florjancyk, J.R. Stevens, Electrochim. Acta 40 (1995) 2251–2258.
[45] J. Przyluski, M. Siekierski, W. Wieczorek, Electrochim. Acta 40 (1995) 2101–2108.
[46] N. Munichandraiah, G. Sivasankar, L.G. Scanlon, R.A. Marsh, J. Appl. Polym. Sci. 65 (1997) 2191–2199.
[47] N. Munichandraiah, L.G. Scanlon, R.A. Marsh, B. Kumar, A.K. Sircar, J. Appl. Electrochem. 25 (1995) 857–863.